might expect appreciable optical resonance when s-polarized light is incident through an $f/1$ lens.

Other microscopic plasma models (based on instability absorption, for example) could be used to calculate the damping factor in addition to the inverse bremsstrahlung model employed here. Indeed, there appear to be a score or more of absorption mechanisms which could, particularly at high intensity, contribute to the damping factor.

What is intended here is to demonstrate heuristically the importance of optical resonance absorption in simple, but reasonably realistic, circumstances. To the extent that future work can provide an exact and complete description of the damping factor as a function of location and time, the approach described here could then provide a reasonably accurate calculation of the absorption of radiant energy by a plasma.

I wish to thank Robert Godwin and Gene McCall for valuable discussions and encouragement. In particular, I am indebted to Dr. Godwin for considerable assistance in the early stages of this work.

*Work performed under the auspices of the U. S. Atomic Energy Commission.

[1]N. G. Denisov, Zh. Eksp. Teor. Fiz. 31, 609 (1956) [Sov. Phys. JETP 4, 544 (1957)]. See also V. L. Ginsburg, *Propagation of Electromagnetic Waves in Plasmas* (Pergamon, New York, 1970), p. 260 ff.

[2]A. D. Piliya, Zh. Tekh. Fiz. 36, 818 (1966) [Sov. Phys. Tech. Phys. 11, 609 (1966)].

[3]A. V. Vinogradov and V. V. Pustavalov, Pis'ma Zh. Eksp. Teor. Fiz. 13, 317 (1971) [JETP Lett. 13, 226 (1971)].

[4]J. P. Freidberg, R. W. Mitchell, R. L. Morse, and L. I. Rudsinski, Phys. Rev. Lett. 28, 795 (1972).

[5]R. P. Godwin, Phys. Rev. Lett. 28, 85 (1972).

[6]M. P. Bachynski and B. W. Gibbs, Can. J. Phys. 49, 3221 (1971).

[7]H. Wolter, in *Handbuch der Physik*, edited by S. Flügge (Springer, Berlin, 1956), Vol. 24, p. 461.

[8]I. Fidone, Nuovo Cimento 30, 666 (1963).

[9]J. W. Shearer, Phys. Fluids 14, 183 (1971).

[10]L. Spitzer, Jr., *Physics of Fully Ionized Gases* (Interscience, New York, 1962), Chap. 5.

[11]V. P. Silin, Zh. Eksp. Teor. Fiz. 47, 2254 (1964) [Sov. Phys. JETP 20, 1510 (1965)].

[12]F. V. Bunkin and A. E. Kazakov, Zh. Eksp. Teor. Fiz. 59, 2233 (1970) [Sov. Phys. JETP 32, 1208 (1971)].

[13]J. W. Shearer and W. S. Barnes, Phys. Rev. Lett. 24, 92 (1970).

[14]A. Boivin and E. Wolf, Phys. Rev. 138, B1561 (1965).

Light Scattering from Weakly Ionized Nonhomogeneous Plasmas

L. Vriens
Philips Research Laboratories, Eindhoven, The Netherlands
(Received 8 February 1973)

Rayleigh scattering is used to obtain the radial gas density and temperature distributions in low-current Ar arcs. A comparison with spectroscopic results indicates large deviations from local thermodynamic equilibrium. The possibilities of determining excited-state density distributions and transition probabilities by Rayleigh scattering are indicated.

The use of light scattering as a diagnostic tool for ionized gases has been confined, so far, chiefly to Thomson scattering by plasmas with a high degree of ionization.[1] Only recently were other applications reported like resonant[2] and near-resonant[3] Rayleigh and vibrational[4] and stimulated[5] Raman scattering.

In this Letter, nonresonant Rayleigh scattering is used as a new technique for determining gas temperatures and densities in nonhomogeneous weakly ionized plasmas. The method is applied to Ar arcs, of length 40 mm, which burn vertically in a quartz tube with inner and outer diameters of 16 and 20 mm, respectively. The cathode is a heated filament; heating is helpful for stabilizing the arcs, which are constricted.

The light-scattering apparatus is schematically shown in Fig. 1. Use of a pulsed non-Q-spoiled ruby laser, giving 0.5 J within 0.34 msec, made the scattered light intensity I_{sc} large enough to be discriminated from the background light of the discharge, while plasma heating is negligible. The intensity of stray light at the laser wavelength was reduced to 0.2% of I_{sc} for 1 atm Ar at room temperature by taking the following precautions: (i) A cylindrical section of height 5.4 mm is cut out from the middle of the tube, to avoid stray light from the quartz wall; (ii) the windows, which have a double antireflection coating, are placed sufficiently far from the scatter-

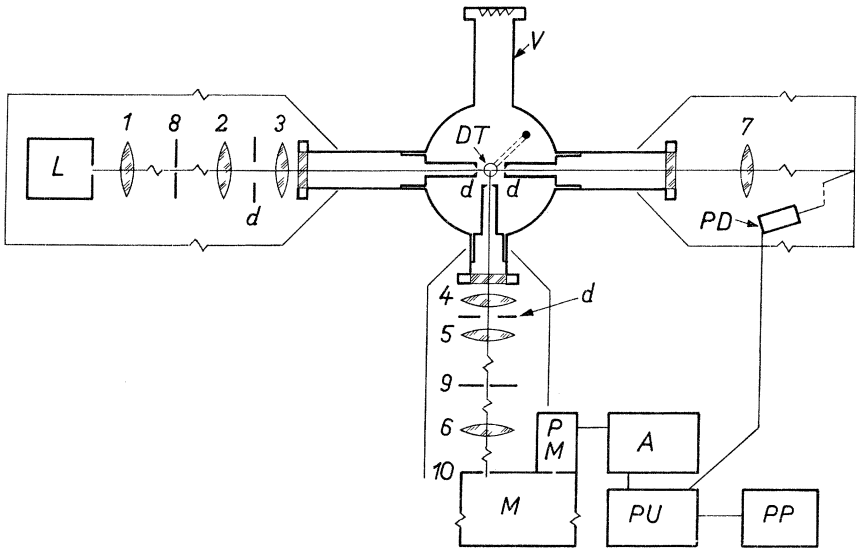

FIG. 1. Schematic diagram of apparatus: L, ruby laser; 1–7, lenses with focal lengths 15, 100, 30, 20, 18, 12, and 15 cm; 8–10, focal-plane stops (8, circular; 9, horizontal; and 10, vertical slit); d, diaphragms; DT, discharge tube; V, vacuum and high-pressure chamber; PD, photodiode; M, 0.5-m grating monochromator; PM, cooled photomultiplier; A, amplifiers; PU, processing unit containing gated integrators, analog to digital converters, and storage memories; PP, printer and puncher.

ing center SC; furthermore, use is made of (iii) diaphragms in entrance and exit tubes, (iv) a light dump opposite the detector, and (v) focal-plane stops in the laser and scattered beams. Because of the opening (i), the tube is placed in a stainless-steel vessel, with diameter 20 cm and height 23 cm, which functions as a vacuum and a high-pressure chamber. Cu seals are utilized for all flanges close to the discharge. The tube is connected to the vertical axis of a magnetically coupled rotary feedthrough, such that the arc can be moved through the SC, in order to measure radial profiles. The spatial resolution is determined by the diameter (0.3 mm) of the laser beam in the SC, by the image (0.3 mm) in this point of the horizontal slit in the scattered beam, and by the image (0.2 to 0.3 mm) of the vertical entrance slit of the monochromator.

The scattered light intensity is given by

$$I_{sc}(r) = I_{in} \sum_j n_j(r) \sigma_j L \, d\Omega, \qquad (1)$$

where r is the radial distance from the axis of the discharge, I_{in} is the intensity of the laser beam, $n_j(r)$ is the local density of the jth plasma constituent, σ_j is its cross section per unit solid angle for scattering at 90° in the plane perpendicular to the polarization direction of the laser beam and in the wavelength band selected, L is the length of the image of the entrance slit of the monochromator on the laser beam, and $d\Omega$ is the solid angle over which light is collected. Furthermore, the pressure which is constant throughout the vessel is given by

$$p = \sum_j n_j(r) k T_j(r), \qquad (2)$$

k being Boltzmann's constant and $T_j(r)$ the "temperature" of the jth plasma constituent.

In this investigation, scattering was measured at the laser wavelength with resolutions between 1.8 and 2.7 Å. The dc current in the Ar arc was varied between 0.6 and 3 A for $p \approx 1$ atm and it was taken at 1 A for $p = 42$ Torr. For these low currents, the electron and excited-state densities are small; quantitative estimates are given further on. Hence, the radial profile of the ground-state atom density $n_0(r)$ is given by the profile of $I_{sc}(r)/I_{in}$ and $p = n_0(r) k T_0(r)$. The absolute calibration results from measuring I_{sc}/I_{in} for 1 atm Ar at room temperature. Density and temperature distributions can thus be obtained directly from the measured $I_{sc}(r)/I_{in}$. Results are shown in Fig. 2. The axis temperatures for 1 atm Ar range from 2900 ± 100 K for 0.6 A up to 4300 ± 150 K for 3 A.

Spectroscopic measurements have been made for comparison purposes. The radial intensity distributions for the spectral lines 7504, 7515, 8408, and 8425 Å are obtained from the mea-

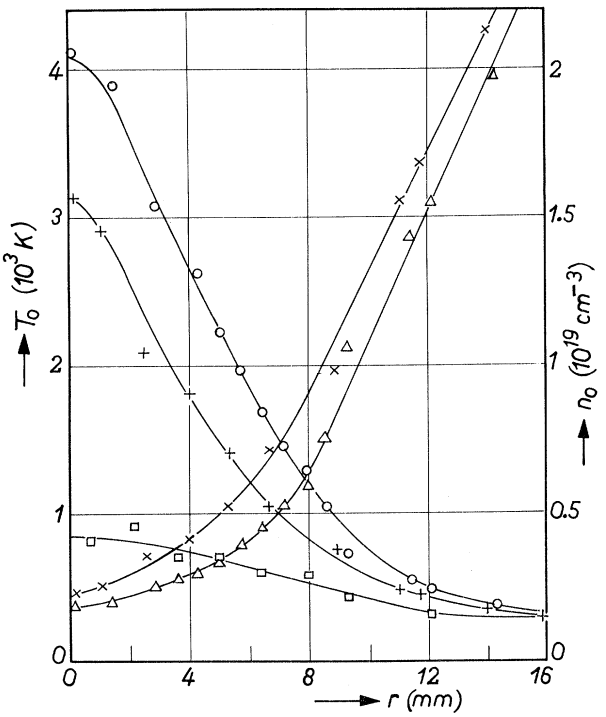

FIG. 2. Measured density n_0 (triangles, crosses) and temperature T_0 (circles, plus signs, squares) distributions for Ar arcs. Triangles and circles, 1.05 atm and 2 A; crosses and plus signs, 1.02 atm and 0.8 A; squares, 42 Torr and 1 A. Characteristic error margins for the axis temperatures are 100 to 150 K.

sured intensity distributions using an Abel inversion technique.[6] For the small excited-state densities worked with, these lines are optically thin. The spatial resolution employed is identical to that used for the light scattering. The axis temperatures found for the 1.02 atm and 0.8-A Ar arc, using the intensity ratios of the 7504- and 7515- and of the 8404- and 8425-Å lines, respectively, assuming local thermodynamic equilibrium (LTE), are 8000 ± 1200 and 9800 ± 800 K, respectively. In contrast, the corresponding gas temperature (see Fig. 2) is 3140 ± 100 K. These values demonstrate the non-LTE character of the plasma. In the analysis of the spectroscopic data use is made of the transition probability ratios $A(7504)/A(7514) = 1.16 \pm 0.05$ and $A(8404)/A(8425) = 1.030 \pm 0.017$. Whereas the individual A values are now known with high accuracy, the ratios obtained from other workers[7-9] agree very well with each other.

The spectroscopically determined temperatures can be used to obtain upper limits of excited-state densities, which when inserted in Eq. (1) yield information on the possible contributions of excited states to I_{sc}. The two levels which will give the largest contributions are the lower levels $4s[\frac{3}{2}]^\circ$ and $4p[\frac{1}{2}]$ of the $\lambda_{1i} = 6965$ and $\lambda_{2i} = 6938$ Å spectral lines, which have different upper levels i. Because of the close vicinity to the ruby-laser wavelength $\lambda = 6943$ Å,

$$\sigma_j = \sigma_{Th} f_{ji}^2 |1 - (\lambda/\lambda_{ji})^2|^{-2}, \quad (3)$$

where $j = 1$ or 2, f_{ji} is the oscillator strength, and $\sigma_{Th} = 7.94 \times 10^{-26}$ cm^2 is the 90° Thomson scattering cross section. The values $f_{1i} = 0.023$ (Ref. 7) and $f_{2i} = 0.0077$ (Ref. 8) yield $\sigma_1 = 12\sigma_{Th}$ and $\sigma_2 = 25\sigma_{Th}$, while $\sigma_0 = 0.0023\sigma_{Th}$. Assuming LTE with $T = 9000$ K yields $(n_1\sigma_1 + n_2\sigma_2)/n_0\sigma_0 = 0.011$. The actual ratio will be much smaller because of the nonvalidity of LTE. For the other currents and pressures worked with, the contributions of excited states can also be disregarded. The spectroscopically determined axis temperatures increase slowly with increasing current. By measuring the wavelength dependence of I_{sc}, it was verified that Thomson scattering is neglibible too.

Finally, we mention some complications and possibilities which arise when the present technique is applied to high-current LTE discharges. (i) The contribution of excited states to I_{sc} may become dominant. For an Ar arc with $T = 18\,000$ K, $(n_1\sigma_1 + n_2\sigma_2)/n_0\sigma_0 = 23$. Because the Thomson scattering signal can be obtained by measuring its wavelength dependence, a weighted radial profile of the excited-state densities $n_1(r)$ and $n_2(r)$ may thus be obtained. (ii) Equation (3) suggests the possibility of measuring radial profiles $n_j(r)$ of selected excited states by near-resonant Rayleigh scattering with tunable dye lasers. (iii) Light scattering further offers the possibility of determining oscillator strength f_{ji} and consequently transition probabilities A_{ij}. One might think in particular of metastable and resonance levels. Their large densities n_j in high-pressure LTE arcs will make near-resonant Rayleigh scattering possible, while self-absorption makes it difficult to obtain these A_{ij} spectroscopically. Near-resonant Rayleigh scattering yields $n_j f_{ji}^2$ [see Eqs. (1) and (3)], while n_j follows from the temperature which can be determined for example from Thomson scattering,[1,10] or spectroscopically from other optically thin lines or from the continuum.

The author wishes to thank J. A. M. Meyer and R. F. Rumphorst for constructing the electronic part of the detection system and C. Mercier for

assistance with some of the measurements.

[1]D. E. Evans and J. Katzenstein, Rep. Progr. Phys. 32, 207 (1969), and references herein.
[2]C. F. Burrell and H. J. Kunze, Phys. Rev. Lett. 28, 1 (1972).
[3]H. Röhr, Z. Phys. 225, 494 (1969).
[4]M. Lapp, L. M. Goldman, and C. M. Penney, Science 175, 1112 (1972).
[5]C. F. Burrell and H. J. Kunze, Phys. Rev. Lett. 29, 1445 (1972).
[6]C. van Trigt, in *Proceedings of the Tenth International Conference on Phenomena in Ionized Gases*, edited by R. N. Franklin (Parsons, Oxford, England, 1971), p. 396.
[7]H. N. Olsen, J. Quant. Spectrosc. Radiat. Transfer 3, 59 (1963).
[8]W. L. Wiese, M. W. Smith, and B. M. Miles, *Atomic Transition Probabilities*, U. S. National Bureau of Standards, National Standards Reference Data Series—22 (U. S. GPO, Washington, D. C., 1969), Vol. 2.
[9]P. J. Dickerman and B. D. Alpiner, J. Quant. Spectrosc. Radiat. Transfer 2, 305 (1962); J. B. Shumaker and C. H. Popenoe, J. Opt. Soc. Amer. 57, 8 (1967).
[10]R. A. Nodwell and G. S. J. P. van der Kamp, Can. J. Phys. 46, 833 (1968); G. Gieres, H. Kempkens, and J. Uhlenbusch, Atomkernenergie 19, 205 (1972).

Anomalous Pinch Effect in a Tokomak

M. N. Bussac, G. Laval, and R. Pellat
Association EURATOM–Commissariat à l'Energie Atomique sur la Fusion, Département de Physique du Plasma et de la Fusion Contrôlée, Centre d'Etudes Nucléaires, 92-Fontenay-aux-Roses, France, and Ecole Polytechnique, Centre de Physique Théorique, Paris V, France
(Received 13 July 1972)

We demonstrate the existence of an anomalous pinch effect if turbulent fields are generated by current instabilities. This effect is similar to the Ware effect, but the stationary electric force is replaced by the drag force resulting from asymmetry of the turbulent fields.

It is now well known[1] that a toroidal electric field can give rise to a radial convection velocity in a geometry of the tokomak type (Fig. 1). Then it is expected that the same effect will occur if the stationary electric force is replaced by the drag force resulting from turbulent fields. However, two conditions must be fulfilled. First, the effective mean free path must be larger than the length of the torus. Second, the turbulence must be generated by the toroidal current density in order to provide an asymmetry of the turbulent fields. Then it is the purpose of this Letter to specify the conditions of instability for a toroidal current carrying plasma, and to demonstrate the existence of an anomalous pinch effect, when these current instabilities are excited. In contrast to recently published works,[2,3] we limit our analysis to the case where

$$\left|\frac{1}{u_0}\frac{\partial u_0}{\partial r}\right| < 4\frac{V_e^2}{c^2}\frac{1}{\lambda_{D_e}}, \frac{V_i}{\Omega_{c_i}}.$$

Here u_0 is the current drift velocity, $V_{e,i}$ are respectively the electron and ion thermal velocities, c the speed of light, λ_D the Debye length, and Ω_{c_i} the ion cyclotron frequency. For simplicity we shall restrict our computations to the banana regime where trapped particles exist, though the results are easily extended to the plateau regime.

It is necessary to inspect again the conditions for instabilities because of the existence of trapped particles which do not carry the current.[4] All of the modes of interest have large parallel wave numbers so that $k_\parallel Rq > 1$, where R is the major radius of the torus and q is the usual safety fac-

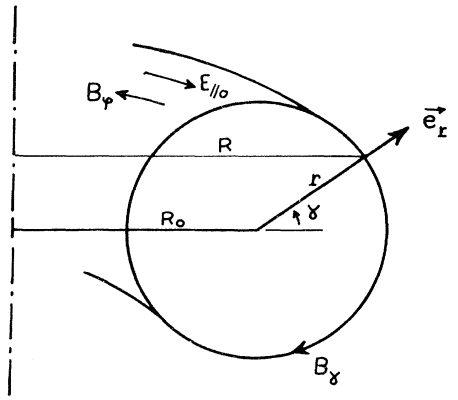

FIG. 1. Coordinate system.